Implementation of Subgrid Cloud Vertical Structure inside a GCM and Its Effect on the Radiation Budget

C. J. STUBENRAUCH

Laboratoire de Météorologie Dynamique, Ecole Polytechnique, Palaiseau, France

A. D. DEL GENIO AND W. B. ROSSOW

NASA/Goddard Space Flight Center, Institute for Space Studies, New York, New York

(Manuscript received 18 July 1995, in final form 15 July 1996)

ABSTRACT

The GISS (Goddard Institute for Space Studies) GCM (general circulation model) predicts stratiform and convective cloud cover and optical thickness at nine atmospheric levels in horizontal grid boxes of 4° lat × 5° long. Until now, the radiative fluxes were calculated once per grid box, assuming clear sky or a complete cloud cover. Here, a refinement of the radiative flux calculation is explored by introducing a horizontal subgrid cloud overlap scheme in which cloud blocks are formed by adjacent cloud layers using maximum overlap. Different cloud blocks are separated by an atmospheric level of clear sky and are assumed to overlap randomly inside the grid box. This subgrid cloud structure allows determination of the occurrence probabilities of columns with different vertical structures inside each horizontal grid box. Then, radiative fluxes are calculated for each of these columns. The radiative fluxes of each horizontal grid box are obtained as the occurrence probability weighted sum of the column fluxes. Compared with the standard GCM version, the horizontal subgrid cloud overlap scheme leads to significant geographical and seasonal changes of the global mean cloud effects on top-of-atmosphere radiative fluxes that are in slightly better agreement with satellite observations. Two extreme assumptions of horizontal cloud size distributions (very small cloud elements or one horizontally continuous cloud) within the cloud blocks are also tested, leading to different column occurrence probabilities. Whereas the global and zonal mean cloud effects on radiative fluxes stay the same, regional differences between the two assumptions (i.e., uncertainties in GCM cloud cover and radiative fluxes produced by a lack of knowledge of subgrid cloud size distributions) can be as large as 15% in cloud cover and 25 (50) W m^{-2} in LW (SW) net fluxes.

The implemented cloud overlap scheme is necessary to study radiative effects of different cloud types separately so that one can better understand the discrepancies in cloud radiative effects between observations and model. This study is not possible with the standard version of the GCM because the instantaneous fluxes do not correspond to realistic cloud structures. But by comparing in more detail the radiative effects of high opaque, cirrus, midlevel, and low clouds with help of the new scheme in GCM and in simultaneous Earth Radiation Budget Experiment and International Satellite Cloud Climatology Project observations, one finds out that high opaque clouds in the GCM have a cloud cover that is too small and are too thin over winter hemisphere ocean, whereas cirrus clouds appear with a cloud cover that is too high. Low clouds in the GCM seem to be too low by about 100 hPa.

1. Introduction

The influence of clouds on the earth's climate is quite complex and, therefore, many studies have been undertaken both with observations and with climate models to get a better understanding of the formation of clouds and their interactions with the dynamics and radiation balance of the atmosphere. The Earth Radiation Budget Experiment has shown more accurately that clouds cool the earth in the global annual mean (Harrison et al. 1990), but regionally and seasonally cloud radiative effects can be quite different, depending on cloud height, thickness, and cloud amount. If one wants to study these cloud-type-dependent radiative effects in more detail with a General Circulation Model (GCM) and eventually compare the results to satellite observations, one has to remember that GCMs have a very coarse spatial resolution of several hundreds of kilometers. At this scale, most GCMs provide or predict cloud cover and optical thickness at different atmospheric levels. To obtain an overall cloud cover for each horizontal grid box that can be compared to satellite observations, these cloud layers have to be horizontally distributed inside the grid box. Several vertical cloud overlap assumptions for midlatitude clouds over oceans were studied using U.S. Air Force cloud observations

Corresponding author address: Dr. Claudia J. Stubenrauch, Laboratoire de Meteorologie Dynamique, Ecole Polytechnique, F-91128 Palaiseau, Cedex, France.
E-mail: stubenrauch@lmdx.polytechnique.fr

over the North Atlantic by Tian and Curry (1989), leading to the conclusion that vertically adjacent cloud layers show a maximum overlap, whereas different cloud types seem to overlap randomly. In cases of different climate regimes within a grid box (e.g., a coastline), it also can happen that different cloud types can be distributed so that their overlap is minimal.

Another study (Yu et al. 1996) has applied hypotheses of maximum and random overlap between GCM cloud layers and evaluated differences in the resulting cloud covers. Whereas the former calculations were done ''off line'' with the results of the LMD (Laboratoire de Météorologie Dynamique) GCM (described first by Sadourny and Laval 1984), we have implemented a horizontal subgrid cloud overlap scheme inside the GISS GCM, so that the resulting fluxes can directly influence the dynamics of the model. By first forming cloud blocks out of adjacent cloud layers (as the analysis of Tian and Curry suggests), we stay in a reasonable range of computing time. The implemented horizontal subgrid cloud overlap scheme and the consequent calculations of occurrence probabilities of columns with different cloud vertical structures inside each horizontal grid box are described in detail in section 2. In the case of random overlap between these cloud blocks, we consider two extreme assumptions of horizontal cloud size distributions (very small cloud elements or one horizontally continuous cloud) within the cloud blocks, leading to different occurrence probabilities. We show the resulting differences in grid box cloud cover between both horizontal cloud size distribution assumptions in section 3. In section 4, we compare cloud cover and cloud radiative effects of the GISS GCM with the implemented horizontal subgrid cloud overlap scheme to those of the standard GISS GCM as well as to some satellite observations. Conclusions are presented in section 5.

2. Method

The GCM at GISS was developed by Hansen et al. (1983), and recently a prognostic cloud water parameterization scheme has been introduced by Del Genio et al. (1996), which provides stratiform and convective cloud cover and interactive optical thickness at 9 atmospheric levels at a spatial resolution of 4° lat × 5° long.

Stratiform clouds are formed when the grid box relative humidity exceeds a prescribed threshold, which is set to 60% at all atmospheric levels relative to an appropriate saturation reference (i.e., with respect to the liquid or ice phase). The resulting stratiform cloud cover then depends on the extent to which the threshold relative humidity is exceeded and the vertical stability of the layer. Cumulus clouds are formed when a parcel of air lifted from one atmospheric level to the next highest atmospheric level is buoyant with respect to the surrounding environment (Del Genio and Yao 1993). The cumulus cloud cover is set equal to the fraction of the layer mass that rises in the convective event, and the latter is determined as that needed to restore the cloud base layer to neutral stability. If the cumulus cloud extends above the 550-hPa level and the stratiform cloud parameterization does not produce cloud above this level, an additional anvil cloud with cover five times that of the cumulus cloud is produced above the 550-hPa level. Cloud optical thickness is calculated from the predicted (and variable) liquid/ice water content, layer vertical extent, and effective particle size with a specified cloud particle number density.

Until now, the radiative fluxes were calculated once per grid box (Lacis and Oinas 1991), assuming clear sky or complete cloud cover. The vertical cloud-layer distribution was obtained by comparing the cloud covers predicted for each atmospheric level to random numbers. If the cloud cover of an atmospheric level was larger than the random number, this particular cloud layer was taken into account for the flux calculation with 100% cloud cover, otherwise it was thrown out. One random number was used for stratiform clouds and another for convective clouds, which means that maximum overlap was assumed within one cloud type and random overlap between stratiform and convective clouds. When both were present at the same atmospheric level, only the stratiform cloud layer was used in the radiative flux calculations. In this way, the varying distribution of vertical cloud cover over the grid box was transformed into a monthly distribution of varying vertical cloud thickness of a completely covered grid box. This method reduces time-consuming radiative flux calculations but still reproduces the monthly mean radiative fluxes. On the other hand, the interaction between radiation and dynamics on timescales shorter than one month is not properly taken into account.

Instead of using random numbers to simulate cloud-layer overlap, other GCMs have attempted to use a parameterization of cloud-layer overlap (Morcrette and Fouquart 1986; Harshvardhan et al. 1987) to produce monthly mean radiative fluxes. But again the flux calculations are done only twice, once for clear sky and once for a completely covered grid box, and the cloudy flux is weighted by a set of probabilities.

In the following, we refine the radiative flux calculation by introducing a horizontal subgrid cloud overlap scheme in which cloud blocks are formed by adjacent cloud layers using maximum overlap. Different cloud blocks are separated by an atmospheric level of clear sky. Stratiform and convective cloud layers are treated independently. Hence, the total number of cloud blocks is the sum of N_s stratiform cloud blocks and N_c convective cloud blocks, $N = N_s + N_c$, and is determined by the number of model layers. Since the GISS GCM has nine atmospheric levels, each of the two cloud types can form at the most five different cloud blocks: $N_s \leq 5$ and $N_c \leq 5$. In the case of the maximum number, each block would be composed of one cloud layer separated

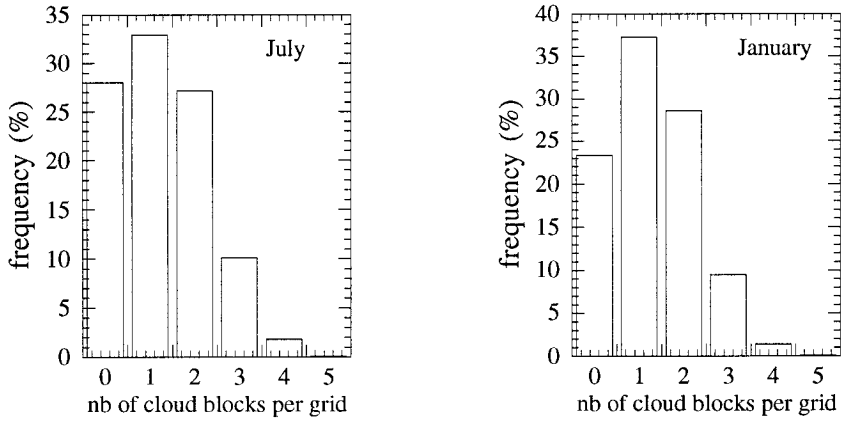

FIG. 1. Frequency distribution of number of cloud blocks per horizontal grid box (a) July and (b) January.

by one atmospheric level of clear sky. Cloud block k is formed of n_k adjacent cloud layers. The N cloud blocks are assumed to overlap randomly inside the grid box, leading to 2^N possible columns inside the grid box with different vertical structures. Then, we calculate the occurrence probabilities of these 2^N possible columns as well as the radiative fluxes for each of these columns. The radiative fluxes of each horizontal grid box are obtained as the occurrence probability weighted sum of the column fluxes. By compositing adjacent cloud layers into N cloud blocks, the column calculations become only about two times more time consuming than the original method. This can be understood by looking at Fig. 1, which shows the frequency distribution in the GCM of cloud block number per horizontal grid box (a) in July and (b) in January. One observes about 60% of cases with 0 or 1 cloud block per grid box (cases taking the same computing time as in the old method), 30% of cases with two cloud blocks leading to at most $2^2 = 4$ times of computing time and about 10% of cases with three cloud blocks leading to at most $2^3 = 8$ times of computing time. Cases with more than three cloud blocks per grid box are quite rare (less than 2%). This doubly time-consuming method is the only possibility leading to instantaneous fluxes that are correct at least in a statistical sense—that is, that have the correct frequency distribution of vertical structures and realistic correlation with short-timescale dynamical variations. This is especially important if using a prognostic cloud parameterization.

We now define horizontal cover, height, and optical thickness for a cloud block before determining overall grid box cloud cover and cloud overlap column probabilities needed for the grid box radiative flux calculation.

a. Characteristics of a cloud block

Cloud block k is formed of n_k adjacent cloud layers. Here, n_k is counted from the highest atmospheric level downward until there is a level with no cloud cover. Maximum vertical overlap is assumed within a cloud block. Stratiform and convective cloud layers are treated separately. The cloud cover of cloud block k is c_k and is determined as the maximum cloud cover of all n_k cloud layers 1 to n_k:

$$c_k = \max(c_1, \ldots, c_{n_k}). \tag{1}$$

The average cloud block top pressure p_k is expressed as the sum of cloud layer pressures from the highest cloud layer 1 to level m_k with the maximum cloud layer cover, each level weighted by the cloud part seen from above:

$$p_k = c_1 p_1 + \sum_{i=1}^{m_k} \max(0, c_i - c_{i+1}) p_i. \tag{2}$$

Finally, the optical thickness τ_k of cloud block k is the layer cloud cover weighted average of the n_k individual cloud-layer optical thicknesses τ_i:

$$\tau_k = \frac{\sum_{i=1}^{n_k} c_i \tau_i}{c_k}. \tag{3}$$

Figure 2 illustrates the variables described above for a cloud block made from three adjacent layers. Only the cloud block cover c_k and the layer optical thicknesses weighted by the ratio of layer cloud cover and cloud block cover are used in the following calculations. In the analysis of section 4c, cloud types are distinguished according to cloud block top pressure p_k.

b. Horizontal cloud block distribution inside a grid box

Here, N randomly distributed cloud blocks inside a grid box lead to 2^N possible columns with different vertical structures. Each column is represented by a vector $(i_1, i_2, \ldots, i_k, \ldots, i_N)$, with $i_k = 1$ if cloud block k is

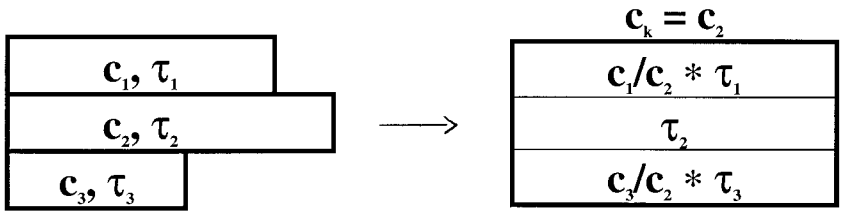

FIG. 2. Illustration of creation of cloud block cover and layer optical thicknesses inside the cloud block used for flux calculations, from three given cloud layers.

present and $i_k = 0$ if cloud block k is absent in this column.

As in the standard GISS GCM, all the following grid box calculations are one-dimensional. Figure 3 illustrates an example of a situation with stratiform cloud covers given at atmospheric levels 2, 3, 8, and 9 and convective cloud covers given at atmospheric levels 5, 6, and 7. In the standard GISS GCM version, only cloud layers for which a random number is smaller than their cloud cover are used for the flux calculation. For example, as illustrated in Fig. 3a, if the two random numbers (here 0.5 for stratiform and 0.3 for convective) were smaller than the cloud cover in atmospheric levels 3, 6, and 9, respectively, the fluxes would be calculated with only these three vertical cloud layers, with 100% cloud cover. The subgrid cloud overlap scheme leads to three cloud blocks as shown in Fig. 3b, numbered from the highest to the lowest: cloud block 1 (with cover c_{s9}) is stratiform consisting of two adjacent cloud layers; cloud block 2 (with cover c_{c6}) is convective, formed by three adjacent cloud layers (hatched); and cloud block 3 (with cover c_{s3}) is stratiform with two cloud layers. In this particular situation, with the horizontal position of the three cloud blocks inside the grid box fixed in order to draw them, the radiative flux has to be calculated for only six columns to obtain the mean flux; namely, the column with cloud blocks 1 and 2 present and cloud block 3 absent and the one with cloud block 3 alone do not occur here, but statistically their probability of occurrence can be nonzero, depending on the different cloud block fractional cover values.

For random vertical overlap between the N cloud blocks, the differential probability dP of occurence of column $(i_1, i_2, \ldots, i_k, \ldots, i_N)$ between the horizontal locations x and $x + dx$ (with $x \in [0,1]$) inside a grid box can be expressed as

$$dP(i_1, i_2, \ldots, i_N)(x) = \prod_{k=1}^{N} g_k(x)\, dx, \qquad (4)$$

where the probability density g_k depends on how each layer cloud cover, given by the GCM, is represented: if they all consist of only one horizontally continuous cloud or if they all are composed of scattered, small clouds. In other words, g_k depends on the cloud size distribution inside each cloud block of the grid box. Since these cloud size distributions are not given by the GCM, one has to make an assumption in order to calculate dP. In general, the g_k's could have many different behaviors inside the grid box, from a constant function to a polynomial of order the number of clouds that form the given cloud block cover. In sections 2b(2) and 2b(1), we will see that in the case of a cloud block made from one single cloud, g_k has partly constant and partly linear behavior, whereas in the case of a cloud block made from a very large number of clouds, g_k has only constant behavior.

The fraction f of each of the 2^N columns inside the grid box, which corresponds to their probability of occurrence, is obtained by integration of $dP(i_1, i_2, \ldots, i_N)$ over the horizontal location x from 0 to 1:

$$f(i_1, i_2, \ldots, i_N) = \int_0^1 dP\,(i_1, i_2, \ldots, i_N)(x). \qquad (5)$$

The clear-sky probability inside a grid box can be obtained by setting all i_k's to 0 in Eq. (5). The total grid box cloud cover, $\langle \text{cov} \rangle$, is then

$$\langle \text{cov} \rangle = 1 - f_{(0, 0, \ldots, 0)}. \qquad (6)$$

The above considerations are valid only under the assumption that the layer cloud covers and optical thicknesses are predicted by the GCM independently in each grid box. Another way to consider the problem is to assume that cloud blocks are always made from horizontally continuous cloud layers but with different boundary conditions at the grid edge. The two extreme cases in which the calculations become simple are discussed in the following: 1) the given layer cloud covers are formed from horizontally very small clouds and 2) the given layer cloud covers represent one horizontally continuous cloud that may be contained wholly within the grid boundaries.

1) ASSUMPTION OF HORIZONTALLY VERY SMALL CLOUDS

For an independent grid box, Fig. 4a illustrates the situation where one cloud block k consists of many horizontally very small clouds. The clear-sky differential probability becomes just $dP_{(0)}(x) = 1 - c_k$, independent of the horizontal location, x, inside the grid box.

Hence, for N cloud blocks, the total grid box cloud cover can be easily calculated as

atmospheric level	stratiform cloud cover	stratiform cloud opt. thickness	convective cloud cover	convective cloud opt. thickness
9	$c_{s9} = 0.7$	τ_{s9}	0	0
8	$c_{s8} = 0.4$	τ_{s8}	0	0
7	0	0	$c_{c7} = 0.2$	τ_{c7}
6	0	0	$c_{c6} = 0.4$	τ_{c6}
5	0	0	$c_{c5} = 0.1$	τ_{c5}
4	0	0	0	0
3	$c_{s3} = 0.6$	τ_{s3}	0	0
2	$c_{s2} = 0.3$	τ_{s2}	0	0
1	0	0	0	0

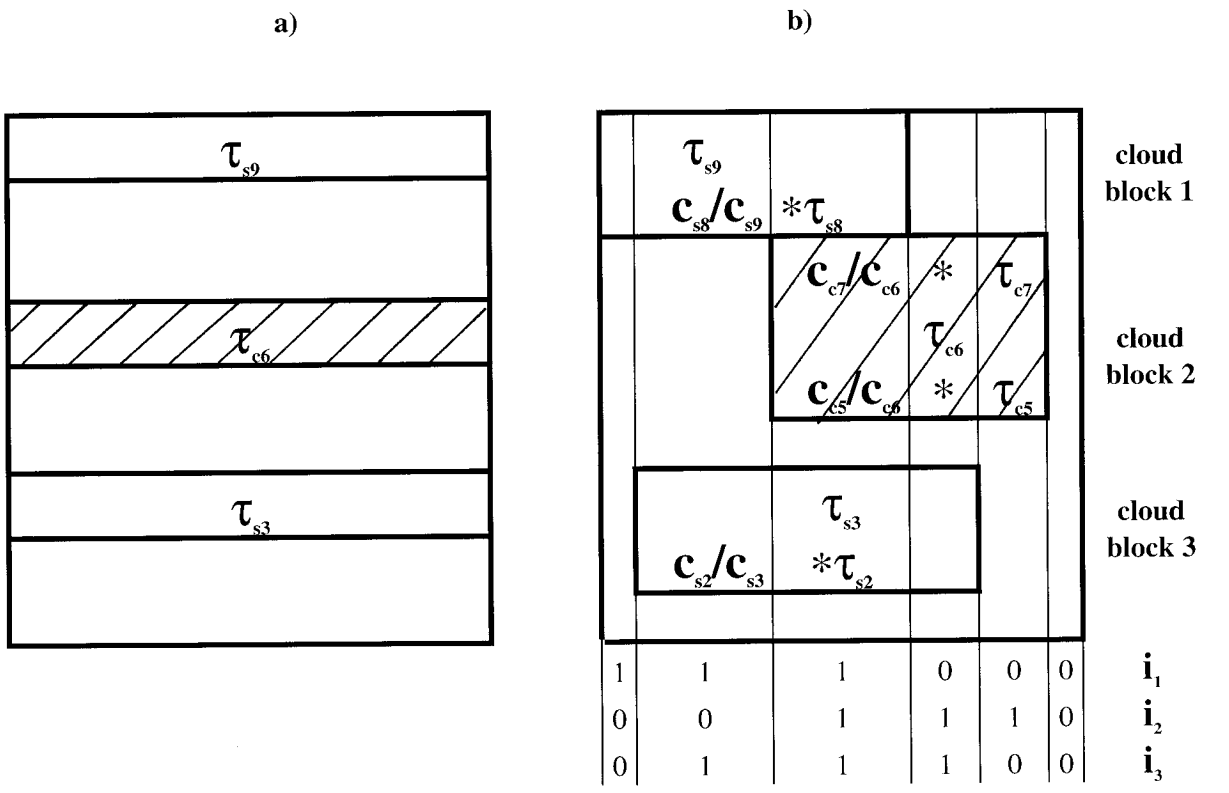

FIG. 3. Illustration of cloud-layer arrangement for radiative flux calculations: example of grid box containing stratiform clouds at four atmospheric levels and convective clouds at three atmospheric levels. (a) Standard GCM: only layers with cloud cover larger than random numbers (here 0.5 for stratiform and 0.3 for convective), shown in bold, taken into account for radiative flux calculations, by covering the whole grid box. (b) New GCM version: all cloud layers taken into account, formed into one convective (hatched) and two stratiform cloud blocks; fluxes are calculated for each column with different vertical overlap conditions.

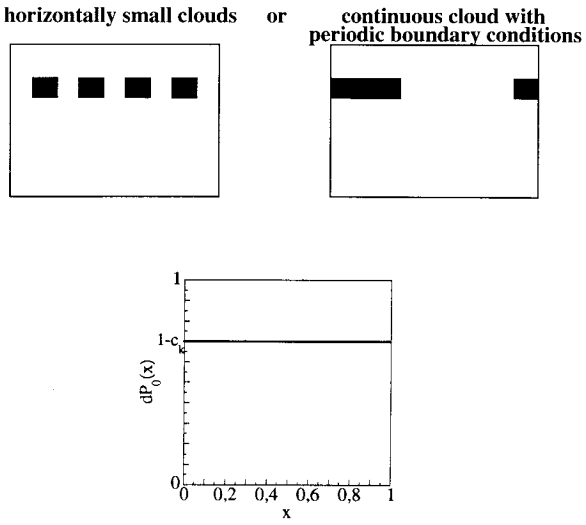

FIG. 4. Clear-sky differential probability as a function of location x inside a grid box, in the case of one cloud block made of horizontally very small clouds (case 1).

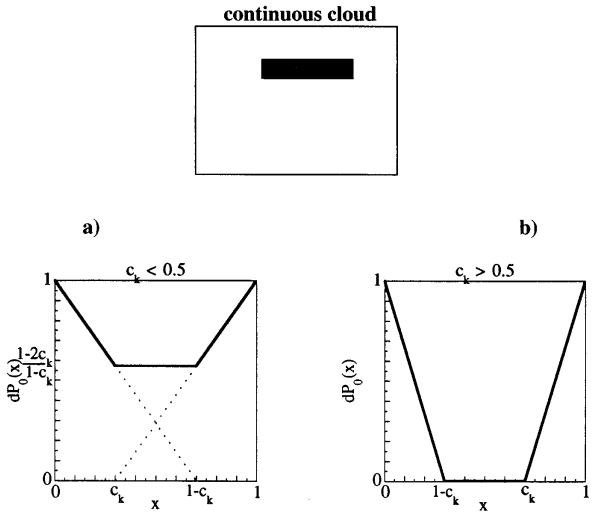

FIG. 5. Clear-sky differential probability as a function of location x inside a grid box, in the case of one cloud block made of one horizontally continuous cloud (case 2): (a) cloud block cover <50%, (b) cloud block cover >50%.

$$\langle \text{cov} \rangle = 1 - \prod_{k=1}^{N} (1 - c_k). \tag{7}$$

The 2^N possible fractions with different vertical structure $(i_1, i_2, \ldots, i_k, \ldots, i_N)$ are then

$$f(i_1, i_2, \ldots, i_N) = \prod_{k=1}^{N} (i_k + (-1)^{ik}(1 - c_k))$$

with

$$i_k = \begin{cases} 1 & \text{if cloud block } k \text{ present} \\ 0 & \text{if cloud block } k \text{ absent.} \end{cases} \tag{8}$$

It so happens that the case of a cloud block k made from one horizontally continuous cloud, but with periodic boundary conditions at the grid box edge, shown in Fig. 4b, gives the same result as above in the calculation of grid box cloud cover and column fractions. This is the most general assumption you can make if you want to analyze clouds from satellite observations (Tian and Curry 1889; Yu et al. 1996) or if you want to calculate grid box cloud covers off line from the GCM layer cloud covers (Yu 1993), because the clouds were already created. Boundary conditions at grid box edges should change only from one climate regime to the next.

On the other hand, if one wants to implement a horizontal subgrid cloud overlap scheme directly inside a GCM, so that the resulting fluxes can directly influence the dynamics of the model, one can hold the view that the cloud covers and optical thicknesses at the different atmospheric levels are predicted by the GCM independently in each grid box. In this case, Fig. 4a shows one extreme case of horizontal cloud size distribution and the other extreme case of horizontal cloud size distribution will be discussed in the following paragraph.

2) ASSUMPTION OF ONE HORIZONTALLY CONTINUOUS CLOUD

Figure 5 illustrates a calculation of the clear-sky differential probability for one cloud block k composed of one horizontally continuous cloud (a) with $c_k < 0.5$ and (b) with $c_k \geq 0.5$. Since the whole cloud has to stay inside the boundaries of the grid box, the probability of clear sky should be higher around the grid box edges than in the middle of the grid box. Instead of $dP_{(0)}(x)$ being constant $(1 - c_k)$ inside the grid box as in case (1), $dP_{(0)}(x)$ is now a linear function of the horizontal location x (in $[0, e_1]$ and $[e_2, 1]$) or constant as in interval $[e_1, e_2]$, with $e_1 = \min(c_k, 1 - c_k)$ and $e_2 = \max(c_k, 1 - c_k)$. One observes that $dP_{(0)}(x)$ is symmetric about $x = 0.5$.

As we have seen in Fig. 5, the differential probability of clear sky $dP_{(0, 0, \ldots, 0)}$ now depends on the horizontal location x inside the grid box. Here, N cloud blocks yield $2*N + 1$ intervals in which the behavior of $dP_{(0, 0, \ldots, 0)}(x)$ can be different (from constant to a polynomial of order the number of cloud blocks). Since $dP_{(0, 0, \ldots, 0)}(x)$ is symmetric about $x = 0.5$, one only has to describe the first half of the shape of dP for the integration over the grid box. The intervals are determined by sorting in increasing order the N values of cloud covers c_k and N values of clear-sky fractions $(1 - c_k)$ into one $2*N$ dimensional array, e. Then, one determines N probability densities g_k for each of the $N + 1$ intervals $[0, e_1], [e_1, e_2], \ldots, [e_{j-1}, e_j], \ldots, [e_N, 0.5]$:

$$g_{k,j}(x) = (i_k + (-1)^{ik}\left(\frac{x}{c_k - 1} + 1\right) \qquad \text{for } x < e_j$$

and

$$g_{k,j}(x) = \left[i_k + (-1)^{ik} \left(\max\left(0, \frac{1 - 2c_k}{1 - c_k}\right)\right)\right] \quad \text{for } x \geq e_j, \tag{9}$$

with

$$i_k = \begin{cases} 1 & \text{if cloud block } k \text{ present} \\ 0 & \text{if cloud block } k \text{ absent.} \end{cases}$$

In Fig. 3, we have $c_1 = 0.7$, $c_2 = 0.4$, and $c_3 = 0.6$, $1 - c_1 = 0.3$, $1 - c_2 = 0.6$, and $1 - c_3 = 0.4$. Therefore, the six-dimensional array e would be (0.3, 0.4, 0.4, 0.6, 0.6, 0.7), and the four intervals for which one has to calculate the three probability densities would be [0, 0.3], [0.3, 0.4], [0.4, 0.4], and [0.4, 0.5]. As one can see in this specific case, only three intervals are to be considered, since the length of one is 0.

For each interval $[0 - e_1]$, $[e_1 - e_2]$, . . .or $[e_N - 0.5]$, there is a unique set of the $g_{k,j}$'s to be used. The fraction of each of the 2^N columns inside the grid box is obtained by integration over x from 0 to 1. To make the integration analytically possible, one has to transform the product of functions $\Pi\ g_{k,j}(x) = \Pi\ (i_k + (-1)^i k(A_{k,j}x + B_{k,j})$ into a series $\Sigma\ D_n\ x^n$, which means that one has to determine $N + 1$ values of D_n from the N values of $A_{k,j}$ and $B_{k,j}$ for each of the $N + 1$ intervals $[e_{j-1}, e_j]$. Then, the integral over x can be resolved as

$$\begin{aligned} f(i_1, i_2, \ldots, i_N) &= 2 \sum_{j=1}^{N+1} \int_{e_{j-1}}^{e_j} dx \prod_{k=1}^{N} g_{k,j}(x) \\ &= 2 \sum_{j=1}^{N+1} \int_{e_{j-1}}^{e_j} \prod_{k=1}^{N} (A_{k,j}x + B_{k,j}) \\ &= 2 \sum_{j=1}^{N+1} \sum_{n=0}^{N} \left(D_{n,j} \frac{{e_{j+1}}^{n+1} - {e_j}^{n+1}}{n + 1}\right), \end{aligned} \tag{10}$$

with

$$A_{k,j} = (-1)^{ik} \frac{1}{c_k - 1}$$

and

$$B_{k,j} = (-1)^{ik} + i_k \qquad \text{for } x < e_j$$

or

$$A_{k,j} = 0$$

and

$$B_{k,j} = (-1)^{ik} \max\left(0, \frac{1 - 2c_k}{1 - c_k}\right) + i_k \quad \text{for } x \geq e_j,$$

with

$$i_k = \begin{cases} 1 & \text{if cloud block } k \text{ present} \\ 0 & \text{if cloud block } k \text{ absent.} \end{cases}$$

For each jth interval, $[e_{j-1}, e_j]$, the $N + 1$ $D_{n,j}$'s are obtained as the sum over the $2N$ columns of products of the different $A_{k,j}$'s and $B_{k,j}$'s, depending upon which of the N cloud blocks are present in each particular column:

$$D_{n,j} = \sum_{m=0}^{2^N - 1} \prod_{k=0}^{N} h_k,$$

with

$$h_k = \begin{cases} A_{k,j} & \text{if cloud block } k \text{ is present in column } m \\ B_{k,j} & \text{if cloud block } k \text{ is absent in column } m. \end{cases} \tag{11}$$

Note that case (1), assumption of horizontally very small clouds, is included in formula (10), if one sets

$$A_{k,j} = 0$$

and

$$B_{k,j} = (-1)^{ik}(1 - c_k) + i_k \quad \text{for } x \in [0, 1].$$

c. Radiative flux calculations inside a grid box

Now, the radiative fluxes are calculated for each of these columns with different overlapping cloud blocks. To obtain the average flux of the grid box, the column fluxes have to be summed up, each flux weighted by the calculated fraction of the corresponding column.

In each column, all cloudy layers i are used in the radiative flux calculations. Each column is supposed to be completely covered by all cloud layers belonging to the corresponding cloud blocks. The optical thickness τ_i of each layer inside a column is then weighted by the ratio of layer cloud cover c_i and cloud block cover c_k: $\tau_i c_i / c_k$ are used in the radiative flux calculations. If in one column, a convective and a stratiform cloud block occur in the same layer, the maximum $(\tau_i c_i)$ is chosen inside this column.

3. Grid box cloud cover comparison between horizontal cloud size assumptions (1) and (2)

We consider the difference in the grid box cloud cover, produced by the opposite extreme assumptions about cloud size distributions. For two cloud blocks present in the grid box, Fig. 6 shows this difference (case 1 − case 2) as a function of the difference between the two cloud block covers $c_1 - c_2$, with c_1 the larger cloud block cover. The figure includes eight curves, for c_1 from 20% to 90%, in steps of 10%. The grid box cloud cover calculated for case 1 (broken cloudiness) is always larger than that calculated for case 2 (continuous layers), with a maximum difference when both cloud block covers are nearly the same, decreasing to zero when the difference between the two blocks is largest. The maximum difference in total cloud cover between the two cases is 11% when both cloud block covers are around 70%.

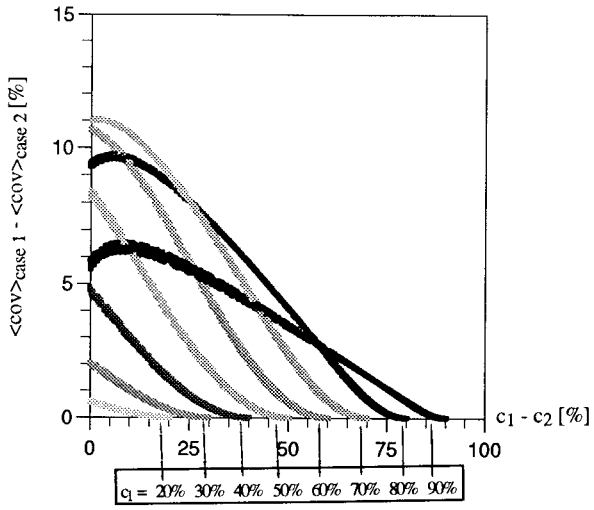

FIG. 6. Situation of two cloud blocks inside a grid box: difference in grid box cloud cover between case 1 and case 2 as a function of cloud block cover difference for maximal cloud block covers c_1 from 20% to 90%, in steps of 10%.

This means that, in the case of random cloud block distribution within a grid box, one has to deal with uncertainties in grid box cloud cover of up to 11%, if one does not know the cloud size distribution inside the grid box.

4. Comparison of cloud radiative effects calculated by the standard GCM and by the GCM with subgrid cloud overlap scheme

a. Global cloud effects on radiative fluxes

The new method has been implemented in the GISS GCM to produce better-correlated instantaneous radiative fluxes than in the standard version of the GISS GCM. The global monthly mean longwave (LW), shortwave (SW), and net cloud radiative forcings for ocean, land, and the whole globe are shown for July 1987 in Table 1 and for January 1988 in Table 2. The different columns of the tables represent the results obtained from the standard version of the GISS GCM and from the new method assuming cloud blocks made from 1) horizontally very small clouds and 2) horizontally continuous clouds. To provide a measure of the natural variability in the model, an additional column shows the results for the same month of the following year obtained from the standard version.

From these tables one can conclude two facts.

1) The results obtained from the new method are considerably different from the results obtained from the standard GCM, using only one radiative flux calculation per grid box. The difference seems to be significant compared to the small difference in cloud radiative forcing of two consecutive years. In July, the new calculations lead to a stronger net cloud radiative cooling by about 8 Wm^{-2} over land, whereas in January the new subgrid cloud overlap schemes produce a slightly smaller net cloud radiative cooling by about 4 Wm^{-2} over ocean. Thus, the new calculations not only change the amount of the global cloud effect on net fluxes but also the seasonal variation over land and over ocean of the global cloud effect. The contrast in cloud effects between July and January becomes larger over land and smaller over ocean. In both months, the difference between land and ocean diminishes in the new calculations. Over the whole globe, the clouds reduce the net radiation by less in January (-29 Wm^{-2}) than in July (-32 Wm^{-2}). The opposite result was obtained with the standard version of the GISS GCM. These differences should result from the interaction between the instantaneous radiative fluxes and the atmospheric dynamics.

2) On a global scale, there is no visible difference in the cloud radiative forcings between the extreme assumptions about horizontal cloud size distributions inside cloud blocks.

TABLE 1. Cloud radiative forcings over ocean, land, and the whole globe in January, predicted by the standard GISS GCM (old) and by the new GCM version with implemented subgrid cloud overlap scheme assuming 1) horizontally very small clouds (clds) and 2) horizontally continuous clouds (blk).

	Old 1988	Old 1987	Small clouds	Cont. cloud	
LW	16.6	16.6	18.2	17.5	
SW	−51.0	−50.5	−51.7	−51.4	Ocean
net	−34.4	−33.9	−33.9	−33.9	
LW	13.2	13.9	14.5	14.9	
SW	−34.2	−35.6	−43.6	−44.1	Land
net	−20.9	−21.7	−29.1	−29.2	
LW	15.5	15.7	16.9	16.6	
SW	−45.3	−45.5	−49.0	−48.9	Global
net	−29.8	−29.8	−32.0	−32.3	

b. Regional comparisons

To understand better where and why these changes occur, we study maps of the average number of cloud blocks per grid box and the average number of cloud

TABLE 2. Cloud radiative forcings over ocean, land, and the whole globe in July, predicted by the standard GISS GCM (old) and by the new GCM version with implemented subgrid cloud overlap scheme assuming 1) horizontally very small clouds (clds) and 2) horizontally continuous clouds (blk).

	Old 1989	Old 1988	Small clouds	Cont. cloud	
LW	15.1	15.2	15.9	15.8	
SW	−58.0	−58.2	−55.0	−54.8	Ocean
net	−42.9	−43.0	−39.1	−38.9	
LW	12.2	12.2	13.1	12.8	
SW	−22.0	−22.3	−22.0	−21.8	Land
net	−9.8	−10.1	−8.9	−9.0	
LW	14.1	14.2	14.9	14.8	
SW	−45.8	−46.1	−43.8	−43.6	Global
net	−31.7	−31.9	−28.9	−28.8	

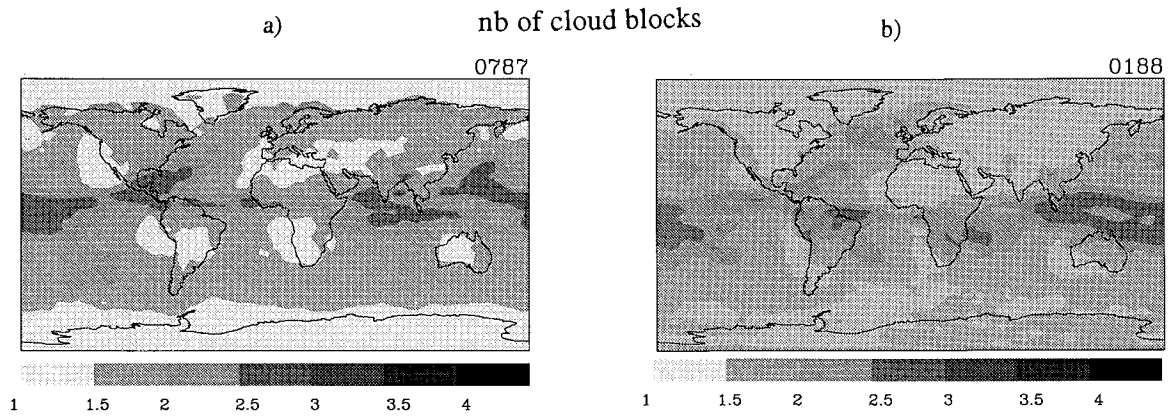

FIG. 7. Geographical map of monthly mean number of cloud blocks inside GCM grid boxes (a) July 1987 and (b) January 1988.

layers per cloud block obtained from the subgrid cloud overlap scheme in the model for July and January. In Figs. 7a and 7b, we observe that in July most grid boxes contain on average two to three cloud blocks. Only the polar regions, the marine stratus regions west of America and Africa, and small land regions in the winter hemisphere are covered mostly by single cloud blocks. The winter hemisphere of January has much more land (North America, Asia, and North Africa) than the winter hemisphere of July, which again is mostly covered by single cloud blocks. Most grid boxes of the relatively small land areas in the Southern Hemisphere are covered by several cloud blocks during summer. We expect the largest differences in the net cloud radiative forcings where there are several cloud blocks in one grid box. Since in July more land is covered by multicloud blocks than in January, there is a large change in cloud radiative effects over land in July.

The cloud block thickness is shown in Figs. 8a and 8b. In both seasons, one observes a distinctive ITCZ with cloud blocks made of three to five cloud layers. The marine stratus and polar clouds are thin, and most other regions have cloud blocks of one to three layers.

By comparing the monthly mean grid box cloud cover from the old version with the two new versions, we find over most land regions in July an increase of cloud amount of up to 25%, North Asia exhibiting the largest change. The northern polar region has less clouds in the new schemes. In January, the differences are more scattered, with the opposite behavior in the polar regions. The regional cloud cover changes lead to changes in regional cloud radiative effects. In general, an increase of cloud cover leads to an increase of LW warming and an increase of SW cooling, the extent of the change also depending on the cloud height. The regional differences between the old and new versions are quite large, compared to the differences between two months of consecutive years calculated with the old version of the GISS GCM. The differences in net cloud radiative forcings are smaller, but they are systematic: the new versions reduce the cloud effects over the ocean during summer, which leads to slightly smaller July–January north–south gradients in cloud radiative forcings (Fig. 9). Regional differences between the two new versions (with horizontally very small clouds and horizontally continuous clouds) reach ± 25 Wm^{-2} in LW and ± 50 Wm^{-2} in SW cloud effects. This means that, even taking into account more carefully the vertical structure of

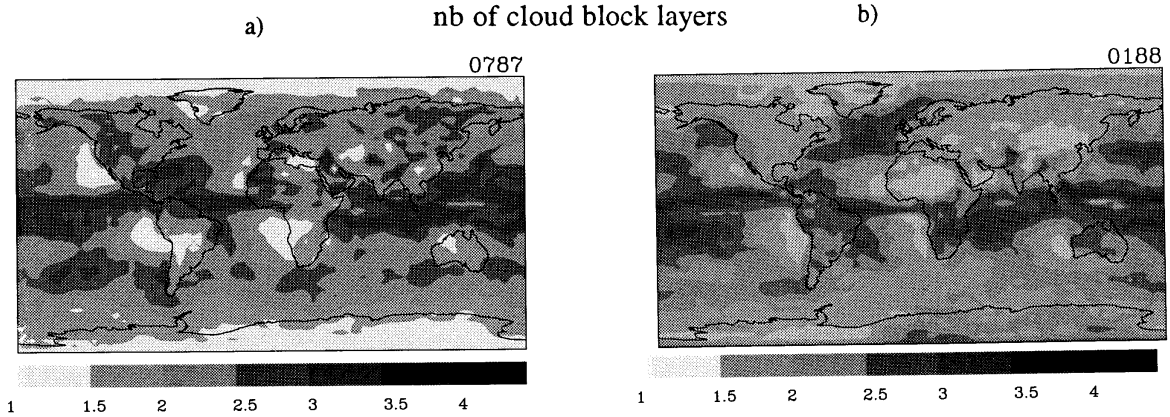

FIG. 8. Geographical map of monthly mean number of cloud block layers inside GCM grid boxes (a) July 1987 and (b) January 1988.

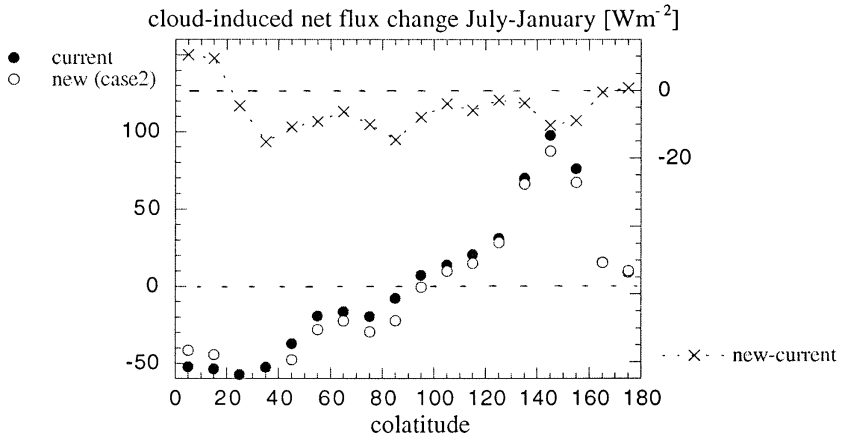

FIG. 9. Zonal net cloud radiative forcing difference between July and January, predicted by the standard GCM (●) and by the new GCM (○), the difference in this seasonal change between the new and standard GCM is indicated as (*x*).

clouds, there remains an uncertainty because of the lack of knowledge of the cloud size distribution within the grid box.

c. Comparisons with satellite observations

To show if the implemented subgrid cloud overlap scheme improves the GCM, we compare cloud cover and cloud radiative forcings to satellite observations. Cloud information is taken from the recently improved ISCCP (International Satellite Cloud Climatology Project) dataset (Rossow et al. 1996), and radiative flux measurements come from ERBE (Barkstrom 1984). We use simultaneous cloud and flux measurements from the polar-orbiting *NOAA-10* satellite, passing the equator at 0730 local time. This is not the best observation time for a global cloud identification, but during July 1987 and January 1988, this is the only satellite working that allows us to combine simultaneous ERBE flux and AVHRR (Advanced Very High Resolution Radiometer) cloud identification measurements. For this comparison, we start with the pixel measurements of both datasets and determine mean fluxes of clear sky and cloudy regions inside grid boxes of $4° \times 5°$, at the same spatial resolution as the GCM.

Figure 10 shows the zonal cloud cover in July and January, separately for ocean (Figs. 10a and 10c) and land (Figs. 10b and 10d), at 0730 local time determined by ISCCP in comparison to the zonal cloud cover predicted by the old GCM version and by the two new GCM versions. Over land, the GCM agrees within 10% with the ISCCP cloud cover, whereas over ocean the GCM cloud cover is too small by about 10% in the Northern Hemisphere up to 30% in the subtropics and in the storm track region of the Southern Hemisphere winter. The implemented subgrid cloud overlap scheme improves slightly the zonal GCM cloud cover compared to the ISCCP cloud cover, especially in July over ocean, where the cloud cover increases by up to 10%, in better agreement to ISCCP, and over the Northern Hemisphere land regions (up to 5%). This fact is encouraging, especially since results obtained by improving only one aspect of the complex GCM calculations do not necessarily get better overall results. The different assumptions of cloud size distribution do not give considerably different zonal results.

In a next step, we study the zonal cloud radiative forcing. Since the *NOAA-10* satellite passes early in the morning, the SW cloud radiative forcing is still small, so that in the following we will concentrate only on the LW cloud radiative forcing. It is calculated from the data as the difference of the monthly mean clear-sky flux inside a $4° \times 5°$ grid box and the monthly mean flux over the same whole grid box. The cloud radiative forcing depends on cloud cover, cloud height, cloud thickness, and frequency of appearance of different cloud types during a month. It also depends on the clear-sky situation. To give a measure of the uncertainty due to the identification of clear sky, we show in Fig. 11 the zonal LW cloud radiative forcing with clear-sky identification from the ERBE method (Wielicki and Green 1989) and in addition the zonal LW cloud radiative forcing with clear-sky identification from ISCCP (Rossow et al. 1993). To minimize misidentification, we examine identified clear-sky regions of $1° \times 1°$ in both datasets. From Fig. 11 we deduce that the uncertainty in zonal LW cloud radiative forcing due to clear-sky identification is only about 5 Wm^{-2}, where the LW cloud forcing with ERBE clear-sky identification is systematically higher. Over land, the GCM LW cloud radiative forcing is in agreement with the data within 10 Wm^{-2}, lower than the data in midlatitudes. Over ocean there is agreement in the Tropics, but especially in the winter midlatitudes the GCM LW cloud radiative forcing is about 20 Wm^{-2} too low. This can be explained by studying geographical maps (not shown) of most frequent

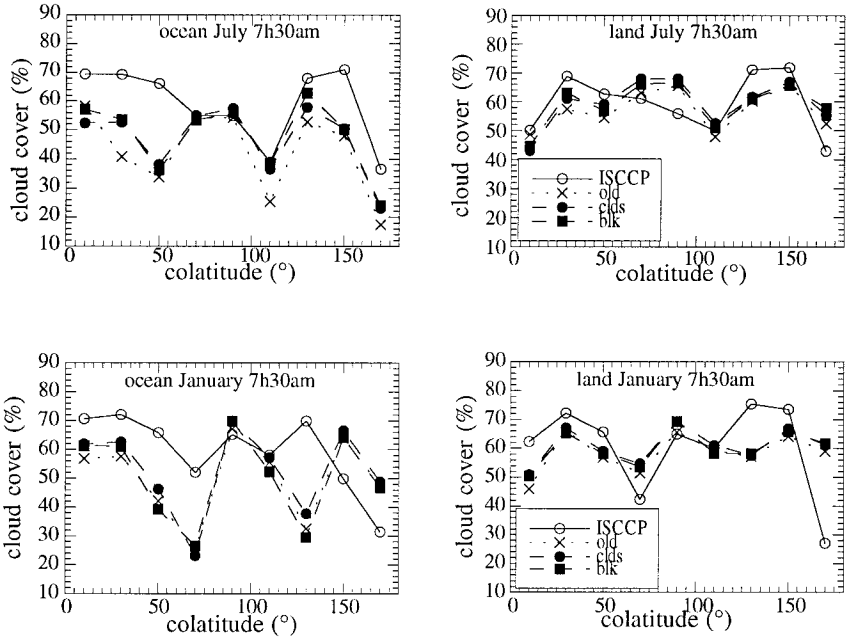

FIG. 10. Comparison of zonal cloud cover predicted by the standard GCM, the new GCM (under both horizontal cloud size assumptions), and zonal cloud cover observed by ISCCP at 0730 LT (data from the *NOAA-10* satellite): (a) ocean July 1987, (b) land July 1987, (c) ocean January 1988, (d) land January 1988.

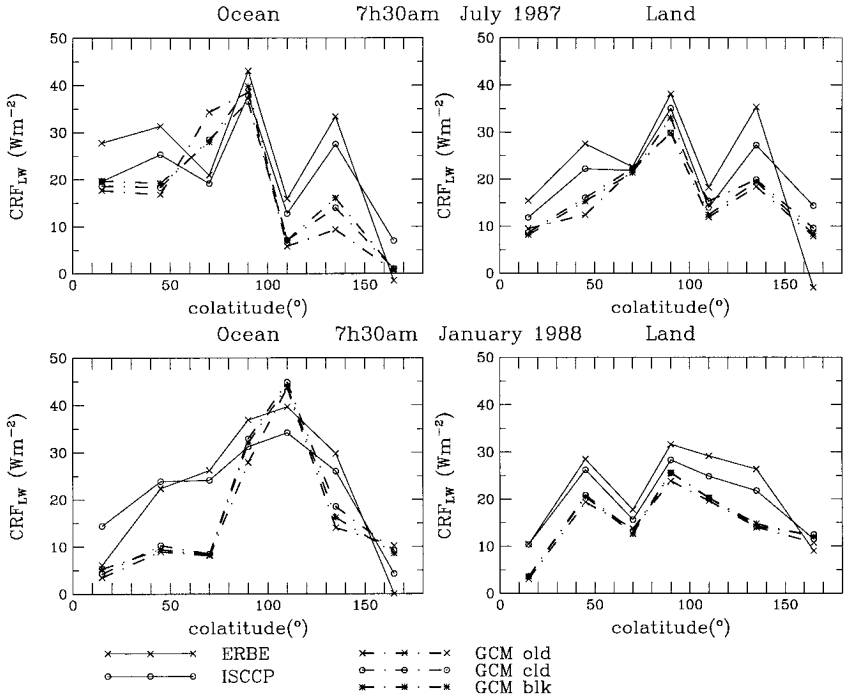

FIG. 11. Comparison of zonal LW cloud radiative forcing (CRF) predicted by the standard GCM, the new GCM (under both horizontal cloud size assumptions), and zonal LW CRF obtained from ERBE flux measurements, with clear-sky detection from ERBE as well as from ISCCP at 0730 (data from the *NOAA-10* satellite): (a) ocean July 1987, (b) land July 1987, (c) ocean January 1988, (d) land January 1988.

clouds types, according to height and optical thickness: the GCM cloudtops are too low in these regions. Again, where the implemented subgrid cloud overlap scheme has increased the cloud cover, the LW cloud radiative forcing is slightly improved, especially over ocean in July. Note that in the subtropical July ocean (around 70° colatitude), where the cloud cover stayed the same, the LW cloud radiative forcing is reduced by more than 5 Wm^{-2}, in better agreement with the data. Considering the geographical maps (not shown) of most frequent cloud types, one observes that in this region the large areas of stratus clouds break down to smaller regions surrounded by cumulus clouds again in better agreement to the data. Reducing the optical thickness reduces the LW cloud radiative forcing.

The implemented subgrid cloud overlap scheme is necessary to analyze zonal cloud radiative forcing separately for different cloud types according to height and optical thickness. This study is not possible with the standard version of the GCM because the instantaneous fluxes do not correspond to a realistic cloud vertical distribution. Due to the large grid box sizes, we characterize cloud type by the most frequent cloud type inside a grid box, as seen from above.

According to ISCCP, high clouds are defined by a cloud-top pressure less than 400 hPa, low-level clouds by a cloud-top pressure larger than 680 hPa, and midlevel clouds have cloud-top pressures in between. The cloud height is determined in two steps by ISCCP: 1) The measured IR radiance together with auxiliary temperature profiles lead to a radiative cloud height. 2) During daytime, the cloud optical thickness is calculated from the measured VIS radiance with a radiative transfer model, taking into account different cloud particle sizes for water and ice clouds (Rossow et al. 1996). Then the cloud height is corrected for semitransparent clouds. In such a way, cirrus clouds (high clouds with optical thickness smaller than 23) can be distinguished from opaque clouds only during the day, which means only in the summer hemisphere by using the early morning *NOAA-10* data.

Figure 12 shows the observed zonal LW cloud forcings of high opaque, cirrus, midlevel, and low-level clouds for July and January, separately for ocean (Figs. 12a and 12c) and land (Figs. 12b and 12d). In this figure one can study the radiative behavior of different cloud types, if they are present. As one can see, high opaque clouds can have a warming effect by as much as 100 Wm^{-2}, the semitransparent cirrus clouds have a smaller warming effect by a factor of 2. Midlevel clouds warm by about 30 Wm^{-2}, whereas low clouds have a negligiable warming effect of less than 10 Wm^{-2}. These can be compared to the GCM predicted zonal LW cloud radiative forcings of high opaque, cirrus, midlevel, and low-level clouds, also shown in Fig. 12. To make direct comparisons to the data, the most frequent cloud type is determined as seen from a satellite. The cloud block with the lowest cloud block pressure is seen completely: its fraction is the cloud block cover. The fraction of a lower cloud block k seen from above (and not hidden by the higher cloud blocks) can be calculated as the sum of fractions with vertical structures $(0, \ldots, 0, i_k, \ldots, i_N)$ from Eq. (8), where all higher cloud blocks should be absent (0) and the cloud blocks below cloud block k can be absent or present. The largest seen cloud block fraction determines the most frequent cloud type inside the grid box, according to the top pressure of this cloud block. Cirrus clouds are defined by high clouds with an optical thickness smaller than 23. Whereas the latitudinal behavior follows roughly the data (higher LW cloud forcing of high opaque clouds in summer hemisphere), one can observe some differences between data and GCM. In general, the LW cloud radiative forcing of the GCM high opaque clouds is smaller (tops too low), and there is less difference between high opaque and cirrus clouds in the GCM. The GCM midlevel clouds over land in the Tropics have a 15 Wm^{-2} less warming effect than the ISCCP midlevel clouds.

In an attempt to understand these differences between the GCM and observations, we show in Fig. 13 the zonal LW cloud radiative forcing divided by the cloud cover (CRFC), corresponding to the difference between average clear-sky flux and average cloudy flux. The difference in cloud radiative forcing of high opaque clouds is nearly gone in the summer hemisphere, and also the cirrus cloud radiative effect is closer to observed. This better agreement shows that the difference in cloud radiative forcing comes from different cloud covers (not shown): in the GCM the cloud cover of high opaque clouds is by about 20% smaller than the observed one (about 95%), whereas the cirrus cloud cover is much larger (about 90%) in the GCM than in the data (about 70%). The midlevel cloud radiative effect difference is reduced over tropical land, suggesting that the GCM midlevel cloud cover in these regions is too small. On the other hand, the radiative effects of low clouds in the winter hemisphere especially over ocean are larger now than those of low clouds in the GCM. This can be explained by looking at the average cloud-top pressure of the different cloud types (not shown): The average cloud-top pressure of ISCCP low clouds is about 100 hPa lower than that of the GCM low clouds. The remaining differences (especially the too small radiative effects of high opaque clouds in the GCM over the winter hemisphere ocean) can be explained by too thin clouds.

It is interesting to note that both extreme cloud size assumptions give essentially the same zonal radiative behavior, with a small difference in the radiative behavior of high opaque clouds: a pronounced difference between Tropics and winter subtropics appears by assuming horizontally continuous cloud blocks. In comparison to the data, one would prefer this assumption in the Tropics with its convective systems, whereas in the subtropics one would expect more broken clouds, prefering the assumption of horizontally small clouds.

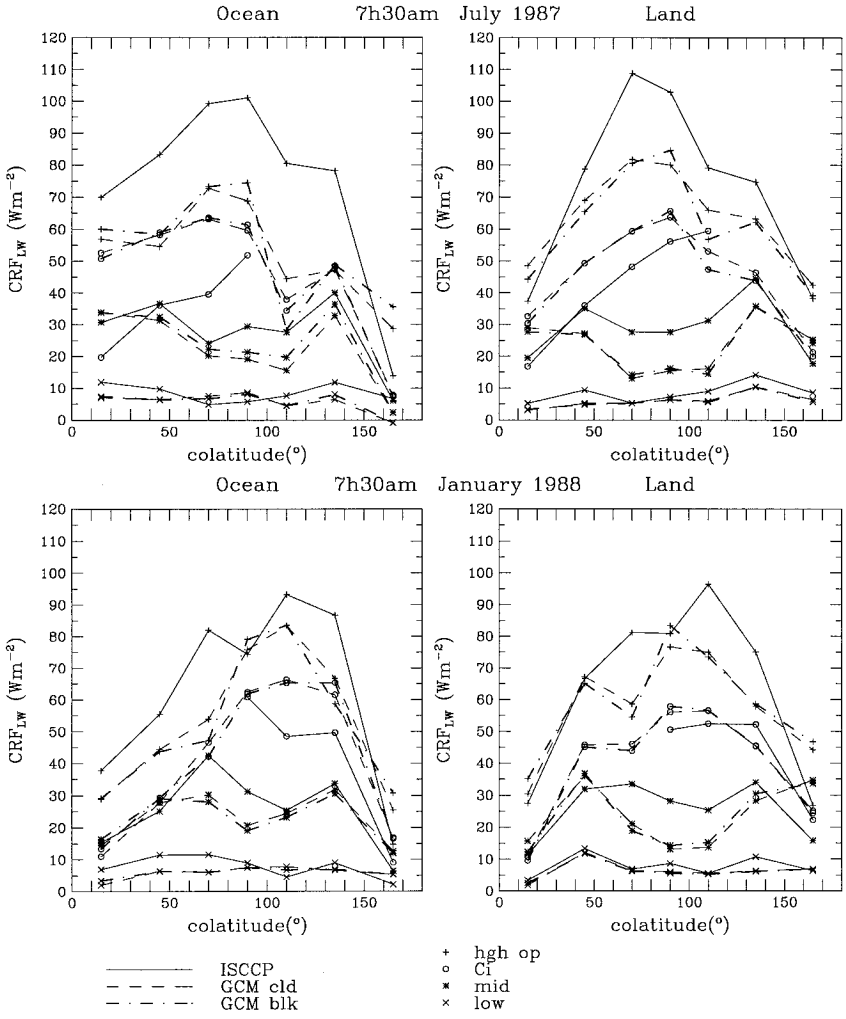

FIG. 12. Comparison of zonal LW cloud radiative forcing (CRF) of different cloud types (high opaque, cirrus, midlevel, and low) predicted by the GCM and zonal LW CRF obtained from ERBE flux measurements, with cloud type identification from ISCCP at 0730 LT (data from the *NOAA-10* satellite). This analysis can be made only with the GCM version with the implemented cloud overlap scheme or with collocated ISCCP-ERBE data: (a) ocean July 1987, (b) land July 1987, (c) ocean January 1988, (d) land January 1988.

5. Conclusions

Most current GCMs do not properly account for cloud vertical structure inside the grid box for radiative calculations. We have presented a subgrid cloud overlap scheme leading to the computation of occurrence probabilities of columns with different vertical structures. By arranging adjacent cloud layers into cloud blocks the computation time increases only approximately by a factor of 2. For this computation, in addition to the layer cloud cover and optical thickness values, an assumption about the horizontal cloud size distribution within the grid box is necessary. Compared with the standard GISS GCM, which uses only one cloud column per calculation, the new scheme with either extreme assumption about horizontal cloud sizes leads to an 8 Wm^{-2} *larger* reduction of net radiative fluxes by clouds over land in July and a 4 Wm^{-2} *smaller* reduction by clouds over ocean in January.

A comparison to satellite observations has shown that the implemented subgrid cloud overlap scheme slightly improves cloud cover and cloud radiative forcing, but improving only one aspect of the complex GCM calculations does not necessarily solve all problems. (For example, it seems that the GISS GCM does not resolve the frontal-scale circulation in midlatitudes that is responsible for much of the observed cloudiness, especially the lifting along the warm front associated with the so-called warm conveyor belt. Or, in the Tropics, where the GISS GCM generally has too much boundary layer cloudiness instead, it apparently underpredicts shallow convection, which removes moisture from the planetary boundary layer, and hence

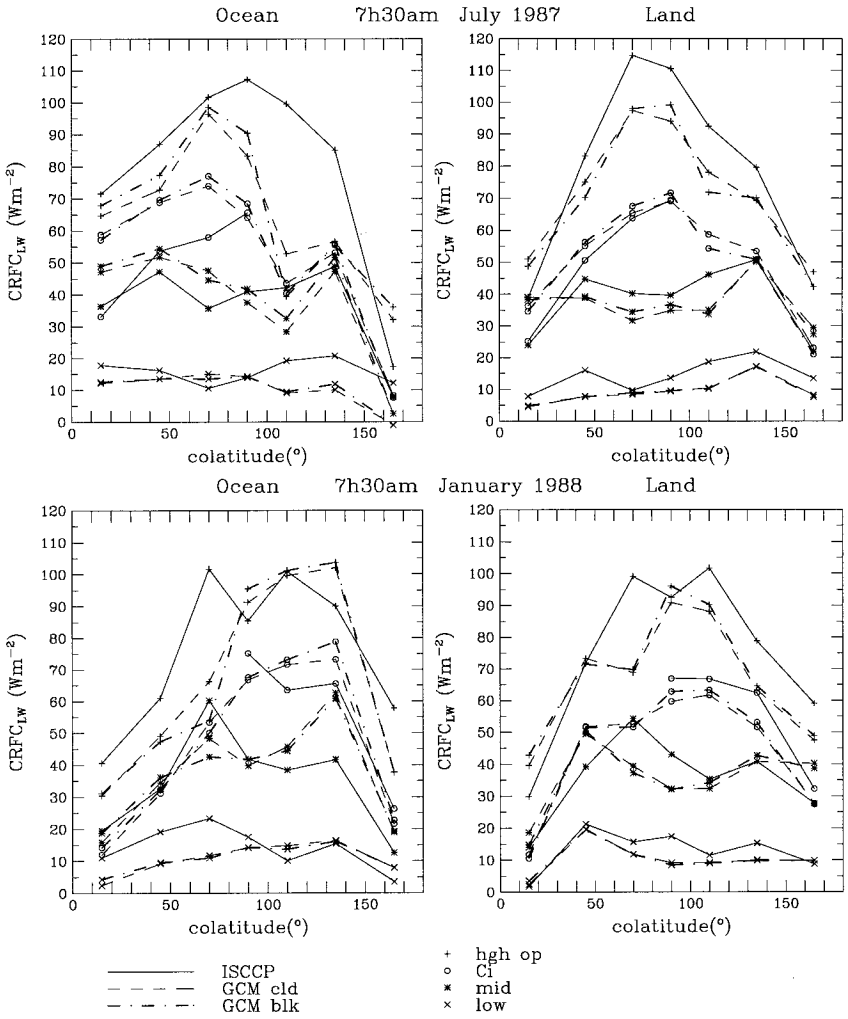

FIG. 13. Comparison of zonal LW cloud radiative forcing divided by cloud cover (CRFC) of different cloud types (high opaque, cirrus, midlevel, and low) predicted by the GCM and zonal LW CRFC obtained from ERBE flux measurements, with cloud-type identification from ISCCP at 0730 LT (data from the *NOAA-10* satellite). This analysis can be made only with the GCM version with the implemented cloud overlap scheme or with collocated ISCCP-ERBE data: (a) ocean July 1987, (b) land July 1987, (c) ocean January 1988, (d) land January 1988.

overpredicts stratiform cloudiness in the parts of the tropical planetary boundary layer that are controlled by trade cumulus.)

Whereas zonal radiative effects seem to be mostly the same, regional uncertainties of up to 10% in total cloud cover, up to 25 Wm^{-2} in LW cloud radiative forcing, and up to 50 Wm^{-2} in SW cloud radiative forcing can still occur if horizontal cloud size distributions vary from region to region. It is interesting to note, that high opaque clouds show a small difference in their zonal radiative behavior: a pronounced difference between Tropics and winter subtropics is produced by assuming horizontally continuous cloud blocks. In comparison to the data, one would prefer this assumption in the Tropics with its convective systems, whereas in the subtropics one would expect more broken clouds, preferring the assumption of horizontally small clouds.

The implemented cloud overlap scheme is necessary to study radiative effects of different cloud types separately so that one can better understand the discrepancies between observations and model. This study is not possible with the standard version of the GCM because the instantaneous fluxes do not correspond to a realistic cloud vertical structure. From this analysis one can conclude that the cloud cover of high opaque clouds seems to be too small in the GCM, whereas cirrus clouds appear in the GCM with a cloud cover that is too large. In addition, high opaque clouds are thinner than the observed high opaque clouds in the winter hemisphere ocean. The cloud cover of midlevel clouds over tropical

land seems to be too small, producing a smaller warming effect than the observed one. Low clouds in the GCM have tops about 100 hPa lower in the atmosphere than low clouds observed by ISCCP.

Acknowledgments. We want to thank A. Lacis for fruitful discussions. Further discussions with O. Boucher and B. Cairns as well as comments by two anonymous reviewers helped to make this analysis more understandable. Technical help with the model calculations was provided by K. Lo and R. Ruedy, and graphics support by J. Jonas.

REFERENCES

Barkstrom, B. R., 1984: The Earth Radiation Budget Experiment (ERBE). *Bull. Amer. Meteor. Soc.,* **65,** 1170–1185.

Del Genio, A. D., and M.-S. Yao, 1993: Efficient cumulus parameterization for long-term climate studies: The GISS scheme. *The Representation of Cumulus Convection in Numerical Models, Meteor. Monogr.,* No. 46, Amer. Meteor. Soc., 181–184.

——, ——, W. Kovari, and K. K.-W. Lo, 1996: A prognostic cloud water parameterization for global climate models. *J. Climate,* **9,** 270–304.

Hansen, J., G. Russell, D. Rind, P. Stone, A. Lacis, S. Lebedeff, R. Ruedy, and L. Travis, 1983: Efficient three-dimensional global models for climate studies: Models I and II. *Mon. Wea. Rev.,* **111,** 609–662.

Harrison, E. F., P. Minnis, B. R. Barkstrom, V. Ramanathan, R. D. Cess, and G. G. Gibson, 1990: Seasonal variation of cloud radiative forcing derived from the Earth Radiation Budget Experiment. *J. Geophys. Res.,* **95,** 18 687–18 703.

Harshvardhan, R. Davies, D. A. Randall, and T. G. Corsetti, 1987: A fast radiation parameterization for atmospheric circulation models. *J. Geophys. Res.,* **92,** 1009–1016.

Lacis, A. A., and V. Oinas, 1991: A description of the correlated *k* distribution method for modeling nongray gaseous absorption, thermal emission, and multiple scattering in vertically inhomogeneous atmospheres. *J. Geophys. Res.,* **96,** 9027–9063.

Morcrette, J.-J., and Y. Fouquart, 1986: The overlapping of cloud layers in shortwave radiation parametrizations. *J. Atmos. Sci.,* **43,** 321–328.

Rossow, W. B., A. W. Walker, and L. C. Garder, 1993: Comparison of ISCCP and other cloud amounts. *J. Climate,* **6,** 2394–2418.

——, ——, D. Beuschel, and M. Roiter, 1996: International Satellite Cloud Climatology Project (ISCCP): Description of new cloud datasets. WMO/TD-No. 737, World Climate Research Programme, Geneva, Switzerland, 115 pp.

Sadourny, R., and K. Laval, 1984: January and July performance of the LMD general circulation model. *New Perspectives in Climate Modelling,* A. Berger and C. Nicolis, Eds., Elsevier, 173–198.

Tian, L., and J. A. Curry, 1989: Cloud overlap statistics. *J. Geophys. Res.,* **94,** 9925–9935.

Wielicki, B. A., and R. N. Green, 1989: Cloud identification for ERBE radiative flux retrieval. *J. Appl. Meteor.,* **28,** 1133–1146.

Yu, W., 1993: Étude comparative des propriétés de la couverture nuageuse observée par satellites et simulée par un modèle du climat. Ph.D. dissertation, University Blaise Pascal, 185 pp.

——, M. Doutriaux, G. Sèze, H. Le Treut, and M. Desbois, 1996: A methodology study of the validation of clouds in GCMs using ISCCP satellite observations. *Climate Dyn.,* **12,** 389–401.